Evaluation of radon absorption and detection properties of a plastic scintillator developed for PSD measurements

Vladislav Todorov, Strahil Georgiev, Matthieu Hamel, Chavdar Dutsov, Benoit Sabot, Ivelina Dimitrova, Krasimir Mitev

Measurement 231 (2024) 114554

Contents lists available at ScienceDirect

Measurement

journal homepage: www.elsevier.com/locate/measurement

Evaluation of radon absorption and detection properties of a plastic scintillator developed for PSD measurements

Vladislav Todorov [a], Strahil Georgiev [a], Matthieu Hamel [b], Chavdar Dutsov [a,1], Benoit Sabot [c], Ivelina Dimitrova [a], Krasimir Mitev [a,*]

[a] Sofia University "St Kliment Ohridski", Faculty of Physics, 5 James Bourchier Blvd., Sofia, 1164, Bulgaria
[b] Universite Paris-Saclay, CEA, LIST, Laboratoire Capteurs et Instrumentation pour la Mesure, Palaiseau, F-91120, France
[c] Universite Paris-Saclay, CEA, LIST, Laboratoire National Henri Becquerel (LNE-LNHB), Palaiseau, F-91120, France

ARTICLE INFO

Keywords:
Plastic scintillators
Pulse shape discrimination (PSD)
Temporal stability
Alpha/beta PSD
Radon

ABSTRACT

In the last decade, significant progress has been made in the development of plastic scintillators (PS) with effective neutron/gamma pulse shape discrimination (PSD). In this study, we investigate a plastic scintillator with remarkable neutron/gamma PSD properties for radon detection and alpha/beta PSD. The PS has outstanding alpha-/beta- PSD, energy resolution, and aging stability. It exhibits radon absorption properties with a diffusion length of 0.224(23) mm and a partition coefficient of 10.6(11) at 20(1) °C. We show how the absorption of radon can enhance studies on the alpha/beta PSD and energy resolution of plastic scintillators. Additionally, we introduce an improved peak shape model for the approximation of the PS's alpha-particle spectrum of ^{222}Rn and its short-lived decay products.

1. Introduction

Since the discovery of the Pulse Shape Discrimination (PSD) properties of organic scintillators in the 1950s, PSD signal processing techniques have become highly attractive due to their ability to separate contributions in the sum energy spectrum of mixed sources (e.g. γ-quanta, neutrons, α-particles, fission fragments etc.) [1–5]. The variation in ionization density leads to a change in the volume density of triplet states, affecting the probability of triplet-triplet annihilation. Consequently, the higher the ionization density of the ionizing particle, the more likely triplet-triplet annihilations become, leading to tailing in the impulse from the detector. It appeared that achieving effective PSD was more accessible with organic crystals and liquid scintillators than with plastic scintillators (PS) [2,5], hindering the development of plastic scintillators for PSD purposes [6]. However, the growing demand for detectors with reliable neutron/gamma discrimination, essential for radiation protection in nuclear facilities and border control against illegal nuclear material trafficking, has spurred the development of plastic scintillators with good PSD (see, for example [7] and references therein). They offer distinct advantages over other organic scintillators [5,6,8], such as low cost, ease of machining, and could be produced in larger pieces. Unlike liquid scintillators, they do not contain toxic or flammable compounds.

The majority of applications for PSD-capable organic scintillators are primarily focused on neutron/gamma discrimination, although some other applications have also emerged. A few research groups have explored the application of alpha/beta PSD using plastic scintillators or plastic scintillation microspheres (PSM). Bagán et al. [9] and Santiago et al. [10] demonstrated that alpha/beta PSD can be achieved with plastic scintillation microspheres. Mitev [11] tested general-purpose plastic scintillators and PSM for measuring ^{222}Rn by alpha/beta PSD, proving the feasibility of the approach, even though the PS used had mediocre PSD. Pelay et al. [12] attempted to develop PSM from polycarbonate and polystyrene with the goal of high ^{222}Rn absorption ability, but the addition of polycarbonate deteriorated the PSD properties of the PSM. More recently, we successfully tested a lab-made PSD plastic [6] coupled to a photomultiplier tube and a labZY nanoPSD [13] for radon measurements [14]. In another study, Morishita et al. [15] were more interested in applications for radiological decontamination. An EJ-299-33 plastic scintillator (Eljen Technology) displayed a moderate Figure of Merit (FoM) value of 0.56 at 256 keVee between 5.5 MeV alphas from ^{241}Am and betas from ^{90}Sr/^{90}Y. Additionally, Morishita et al. [16] proposed a prototype of a radon detector with alpha/beta discrimination, but they used a stilbene crystal. Hajagos et al. [17] synthesized a highly soluble and polymerizable diphenylanthracene-based dye for plastic scintillators. Samples fabricated using this dye

* Corresponding author.
E-mail address: kmitev@phys.uni-sofia.bg (K. Mitev).
[1] Present address: Paul Scherrer Institute, Villigen PSI, 5232, Switzerland.

https://doi.org/10.1016/j.measurement.2024.114554
Received 12 January 2024; Received in revised form 11 March 2024; Accepted 21 March 2024
Available online 26 March 2024

monomer were found to be hard, durable, and highly transparent. While the ultimate performance of their new material was just below the threshold limit for usability in real detectors [17], the authors concluded that it can serve as a proof-of-concept for the possibility of highly loaded plastics stabilized via copolymerization, and thus to open possibilities for entirely new classes of dyes for PSD capable PS [17]. Thus, the quest for a plastic scintillator with ideal alpha/beta PSD properties suitable for radon detection is still ongoing.

An important feature of plastic scintillators, particularly when applied for radon measurement, is their ability to absorb radon from the ambient media and concentrate it within their volume. The process of absorption is well-studied and theoretically modeled, enabling the characterization of the radon-absorption properties of plastic scintillators. This modeling also allows for a quantitative correlation between the absorbed radon and the radon in the surrounding media [11,18–20]. The absorption of ^{222}Rn leads to increased detection efficiency and enables alpha-spectrum analysis since the source is situated inside the scintillator [14]. On the other hand, because radon and its short-lived decay products are alpha and beta emitters, the absorbed radon becomes an ideal alpha/beta source for characterizing the PSD properties of plastic scintillators.

This work presents a recently developed plastic scintillator (PS) with excellent neutron/gamma discrimination properties. The study showcases its temporal stability and investigates its radon absorption characteristics, including the determination of its partition coefficient K and diffusion length L_D over a 4+ years lifespan. Additionally, it is demonstrated how ^{222}Rn is employed to examine the scintillator's alpha/beta PSD and energy resolution. A robust fitting function for analyzing the peaks in the alpha- spectrum obtained after PSD is proposed.

2. Methods and materials

2.1. Development and properties of alpha/beta pulse shape discriminating plastic

The neutron/gamma PSD features of the plastic scintillator we described in [14] are obtained according to the highly-concentrated primary fluorophore strategy [21]. Here the primary fluorophore is biphenyl and the matrix is cross-linked with a dimethacrylate. This cross-linking process is paramount as it guarantees high durability with time and radiation aging [22]. The composition of the scintillator is styrene 67.2%, 1,4-butanediol dimethacrylate 16.8%, biphenyl 14.3%, p-terphenyl 1.7%, 1,4-bis(5-phenyl-2-oxazolyl)benzene (POPOP) 0.1%. All chemicals were mixed and the liquid solution was saturated with argon and five freeze-pump-thaw cycles were performed prior to polymerization. The thermally-initiated, radical polymerization was conducted by heating under a neutral atmosphere the liquid monomeric solution with fluorophores. The temperature was slowly increased from 60 to 140 °C to balance between high-rate polymerization and avoiding bubbles creation. Usually full polymerization was reached in less than two months. Once the polymerization was finished, the as-prepared scintillator was cut and polished, giving its final shape. Here the scintillator has a diameter of 30 mm and a thickness of 12 mm. Hereafter, this plastic scintillator will be referred to as "PSDplastic". It is the same PS as was used in Ref. [14].

2.2. Study of ^{222}Rn absorption in the scintillator

A model that describes the absorption of radioactive noble gases (RNGs) in polymer materials is presented in [18]. It is assumed that once a polymer specimen is immersed in RNG-containing media, the RNG atoms are adsorbed at the surface of the polymer and an equilibrium between the RNG concentration in the polymer (C_{in}) and in the ambient media (C_{out}) is promptly reached. The equilibrium is characterized by the partition coefficient $K = C_{in}/C_{out}$. For some polymers $K \gg 1$ which makes them very suitable RNG samplers. Once adsorbed, the RNG transport in the polymer is described by the diffusion equation with an additional term that accounts for radioactive decay:

$$\frac{\partial c}{\partial t} = D\left(\frac{\partial^2 c}{\partial x^2} + \frac{\partial^2 c}{\partial y^2} + \frac{\partial^2 c}{\partial z^2}\right) - \lambda c, \tag{1}$$

where c is the RNG concentration in the polymer, (x, y, z) and t are space and time variables, D is the diffusion coefficient of the noble gas atoms in the polymer and λ is the RNG decay constant. In [18,19] Eq. (1) is solved considering various specimen shapes and exposure conditions. In the present work thin, parallel-plate scintillator specimens were exposed to ^{222}Rn in air with exponentially decreasing concentration $C_{out} = C_0 e^{-\lambda_{eff} t_s}$ for time t_s and then left to degas in radon-free air for time t_d, where λ_{eff} describes the exponential decrease of the initial activity concentration C_0 of ^{222}Rn in the air. In this case the activity of ^{222}Rn in the specimen is [18]:

$$A(t_s, t_d) = \frac{8\lambda L_D^2 V K C_0}{L^2} \sum_{k=0}^{\infty} \frac{e^{-\lambda_{eff} t_s} - e^{-\lambda_k t_s}}{\lambda_k - \lambda_{eff}} e^{-\lambda_k t_d}, \tag{2}$$

with

$$\lambda_k = \lambda\left(1 + \left(\frac{(2k+1)\pi L_D}{L}\right)^2\right), \tag{3}$$

where L is the thickness and V is the volume of the specimen and $L_D = \sqrt{D/\lambda}$ is the diffusion length of ^{222}Rn in the polymer. The partition coefficient K and the diffusion length L_D (or the diffusion coefficient D) are the only two parameters needed for the practical application of the model.

Based on the model, several approaches for estimation of K and L_D were proposed [12,20,23–27]. Generally, they follow these basic steps:

- Specimens with known dimensions are exposed in RNG-containing media at controlled conditions (e.g. activity concentration, exposure duration, temperature);
- The specimens are left to degas in RNG-free air and the RNG activity in the specimens is measured repeatedly, in order to obtain an experimental follow up of the time-decrease of the absorbed activity $A_i(t_{d,i})$;
- The obtained experimental data $A_i(t_{d,i})$ is fitted with theoretical function given by Eq. (2) as the infinite sum is restricted to a reasonable number of terms [20,27].

2.3. PSD measurement setups

The experimental system used to study the PSD capabilities of the PSDplastic is named Polyphemus 1 (see Fig. 1). This detector features a Hamamatsu R7600U-200 photomultiplier tube. The outer body and optical chamber of the detector are 3D printed with polylactic acid. The shape of the optical chamber is optimized to collect most of the scintillation photons on the photocathode of the PMT. The walls of the chamber are covered with 3M Enhanced Specular Reflector (3M ESR) in order to decrease the number of photons absorbed in the walls. The cavity in which the PS piece is placed was designed to facilitate the radon absorption studies.

The signals from the PMT are processed with the nanoPSD analyzer [13]. With the nanoPSD it is possible to simultaneously acquire four spectra: Time-Invariant Pulse-shape Signatures (TIPS) spectrum, the raw pulse-height spectrum and the separated pulse-height spectra of the alpha and beta particles. The pulse-shape discrimination algorithm of the nanoPSD implements ballistic deficit measurement [28] and the digital pulse-shaping system is time-invariant and operates in real time. The PMT signals are passed through slow and fast shapers. The pulse-height of the slow and fast shapes is measured using peak detectors. The TIPS is the ratio of the maximum of the slow shaper and the maximum of the fast shaper [28].

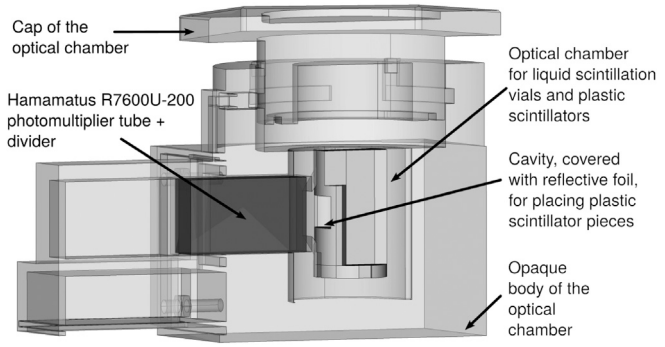

Fig. 1. A cross-section of the Polyphemus 1 detector.

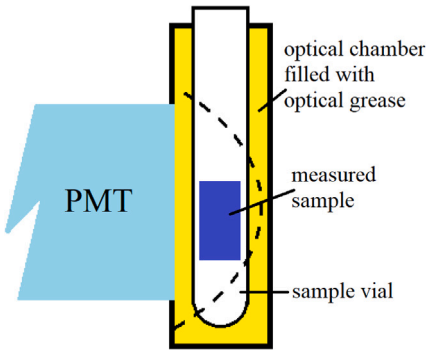

Fig. 2. Cross-section of the PERALS-spectrometer used for the PSD studies.

The system shown in Fig. 1 has excellent capabilities for PSD measurements but the energy resolution is not at its optimum. It is sufficient for the evaluation of the diffusion length of ^{222}Rn in the PS which is based on the ^{214}Po α-peak but the peaks of ^{222}Rn and ^{218}Po are not well separated. This problem has been addressed by gluing the PS piece in the center of the PMT window with silicon optical grease. The sides of the PS piece were covered with reflective foil. These steps significantly improved the energy resolution.

Alongside the newly developed system, measurements of the studied PS were conducted using a commercial spectrometer – Photon Electron-Rejecting Alpha Liquid Scintillation (PERALS) designed for PSD applications [29]. A schematic view of this spectrometer is presented in Fig. 2. The results obtained with this spectrometer served as a benchmark for those acquired with the Polyphemus 1.

2.4. Alpha-spectra analysis

The Polyphemus 1 spectrometer has an excellent capability for PSD measurements provided by the PSDplastic and the nanoPSD analyzer. This allows a complete separation between the α-particle pulses and the pulses due to β-particles or external γ-radiation. Thus, we can obtain the alpha spectrum of ^{222}Rn and its short-lived decay products ^{218}Po and ^{214}Po.

One of the main parameters of the alpha- spectra that was analyzed was the energy resolution (R) of the alpha peaks, defined as:

$$R = 100\frac{\mathrm{FWHM}}{E} \quad [\%] \tag{4}$$

where FWHM is the full width at half maximum of the peak (in keV), and E is the energy (in keV) that corresponds to the centroid of the peak.

Generally, α-peaks have a Gaussian-like shape which arises from the sum of small random fluctuations in the detector system. This suggests that the α-peaks could be approximated by a Gaussian distribution:

$$G(x;\mu,\sigma) = \frac{A}{\sqrt{2\pi\sigma^2}} e^{-\frac{(x-\mu)^2}{2\sigma^2}}, \tag{5}$$

where A is the area, μ is the centroid and σ^2 is the variance of this distribution. In some cases, however, various factors can lead to an asymmetric broadening of the α-peaks (see, for example, [30]).

In [31], it is demonstrated that a significant contributor to the asymmetry of α-peaks in measurements with plastic scintillators is the non-uniformity of the photocathode response of the PMTs. A new function for fitting α-peaks was proposed which consists of a sum of three Exponentially Modified Gaussian (EMG) distributions with three left-handed and one right-handed exponential term. For a single α-peak, the model can be expressed as [31]:

$$\begin{aligned}\tilde{F}(x) = A\Bigg(&\eta_0\frac{\tau_0}{2}\exp\left[\tau_0\left(\mu - x + \frac{\tau_0\sigma^2}{2}\right)\right]\mathrm{erfc}\left(\frac{\mu+\tau_0\sigma^2 - x}{\sqrt{2}\sigma}\right) + \\ &\sum_{i=1}^{3}\eta_i\frac{\tau_i}{2}\exp\left[\tau_i\left(x - \mu + \frac{\tau_i\sigma^2}{2}\right)\right]\mathrm{erfc}\left(\frac{x+\tau_i\sigma^2-\mu}{\sqrt{2}\sigma}\right)\Bigg),\end{aligned} \tag{6}$$

where A, μ and σ^2 are as defined above, τ_i are the exponential coefficients and η_i are the weights of the different terms, which satisfy the normalization condition [31]:

$$\sum_{i=0}^{3}\eta_i = 1 \tag{7}$$

In [31] the weights η_i are restricted to positive values only, as their negative values are considered non-physical. Thus the model describing the three α-peaks in the spectrum of ^{222}Rn and its decay products is:

$$\begin{aligned}F^{+}_{12exp} = &\tilde{F}_{^{222}\mathrm{Rn}}(x;A_1,\mu_1,\sigma_1,\eta_i,\tau_j) + \\ &\tilde{F}_{^{218}\mathrm{Po}}(x;A_1k,\mu_2,\sigma_2,\eta_i,\tau_j) + \\ &\tilde{F}_{^{214}\mathrm{Po}}(x;A_2,\mu_3,\sigma_3,\eta_i,\tau_j), \\ &i=[0,11],\ j=[0,11]\end{aligned} \tag{8}$$

where each F^{+} is a sum of three functions $\tilde{F}$ defined in (6), A_1 is the sum of the areas of ^{218}Po and ^{222}Rn α-peaks, and $k = \frac{I_{^{218}Po}}{I_{^{222}Rn}} = 1.001$ is the equilibrium ratio of the emission rates of ^{218}Po 6.002 MeV α-particles and ^{222}Rn 5.489 MeV α-particles [32].

The above model is further refined in this work. Assuming that the physical processes that lead to the asymmetry of the α-peaks are the same for all three peaks, we can expect that the exponential coefficients in Eq. (8) should be equal for all α-peaks:

$$\begin{aligned}F^{+}_{4exp} = &\tilde{F}_{^{222}\mathrm{Rn}}(x;A_1,\mu_1,\sigma_1,\eta_i,\tau_j) + \\ &\tilde{F}_{^{218}\mathrm{Po}}(x;A_1k,\mu_2,\sigma_2,\eta_i,\tau_j) + \\ &\tilde{F}_{^{214}\mathrm{Po}}(x;A_2,\mu_3,\sigma_3,\eta_i,\tau_j), \\ &i=[0,11],\ j=[0,3]\end{aligned} \tag{9}$$

The difference between Eqs. (8) and (9) is that in the former there are 12 exponential coefficients τ_j ($j = [0,11]$), while in the latter there are 4 τ_j ($j = [0,3]$). Thus, there is a large decrease in the number of exponential parameters in the description of the α-spectra.

In order to compare both models for the approximation of the α-spectra of ^{222}Rn and its decay products, statistical criteria are employed to evaluate the goodness-of-fit. One of these criteria is χ^2, which is defined as [33]:

$$\chi^2 = \sum_{i=1}^{N}\left(\frac{y_i - y(x_i;a_1\ldots a_M)}{\sigma_i}\right)^2, \tag{10}$$

where N is the number of experimental points and M is the number of parameters. Assuming that y_i follow a Poisson distribution one gets:

$$\sigma_i^2 = y_i \tag{11}$$

Using Eq (11) with Eq. (10) gives:

$$\chi^2 = \sum_{i=1}^{N} \frac{\left(y_i - y(x_i; a_1 \dots a_M)\right)^2}{y_i} \tag{12}$$

The reduced χ^2 is defined as:

$$\chi^2_{red} = \frac{\chi^2}{N-M} = \frac{\chi^2}{dof}\,. \tag{13}$$

Additionally, two criteria are used to find the model with the optimal number of parameters. These are AIC (Akaike Information Criterion) and BIC (Bayesian Information Criterion) which are defined as [34,35]:

$$AIC = -2\ln(\mathcal{L}) + 2M \tag{14}$$

$$BIC = -2\ln(\mathcal{L}) + M\ln(N) \tag{15}$$

where $\mathcal{L}$ is the likelihood function of the model. Assuming that the model and data errors are sampled from a normal distribution, the two information criteria (14) and (15) can be written as:

$$AIC = N\ln(\chi^2/N) + 2M \tag{16}$$

$$BIC = N\ln(\chi^2/N) + M\ln(N) \tag{17}$$

When comparing the models, more informative is the difference between the values of AIC and BIC of the current model and the values of the best candidate model, i.e. the model with lowest values of AIC and BIC:

$$\Delta_i(AIC) = AIC_i - \min(AIC) \tag{18}$$

$$\Delta_i(BIC) = BIC_i - \min(BIC) \tag{19}$$

In this way, the most likelihood model from a given group could be determined. However, the criteria do not give information about the absolute likelihood so a better model outside the studied group might exist. Thus defined in Eqs. (18) and (19), the differences between the models can further be used to calculate the Akaike weights defined by [34]:

$$w_i(AIC) = \frac{\exp\left(-\frac{1}{2}\Delta_i(AIC)\right)}{\sum_{r=1}^{R}\exp\left(-\frac{1}{2}\Delta_r(AIC)\right)}\,, \tag{20}$$

where r are the indexes of all studied models. A given weight $w_i(AIC)$ is taken as evidence in favor of a model and can be interpreted as the probability that the model is the most plausible one. All weights are normalized to 1. The weights $w_i(BIC)$ are defined in a similar way:

$$w_i(BIC) = \frac{\exp\left(-\frac{1}{2}\Delta_i(BIC)\right)}{\sum_{r=1}^{R}\exp\left(-\frac{1}{2}\Delta_r(BIC)\right)}\,. \tag{21}$$

3. Experimental

In order to study the PSD and the radon absorption properties of the PSDplastic, rectangular pieces (12 mm × 14 mm with thicknesses specified further in the text) of the scintillator were cut, polished and then exposed to radon. Due to the specifics of the PSD and alpha-spectra analysis, some additional samples of the PSDplastic (described in the text) were also prepared and exposed. To study the potential aging effect on the radon absorption properties of the PSDplastic, two identical experiments were carried out in October 2020 and November 2023 with the experimental setup schematically shown in Fig. 3. The PSDplastic samples along with some Makrofol N foils were placed in a small exposure vessel (180 mL drechsel bottle). Radon from a ^{226}Ra emanation source was promptly introduced in the drechsel and then the inlet and the outlet of the drechsel were sealed. In this way a high radon concentration (about 100 MBq/m^3) was achieved in the exposure vessel. During the exposure the drechsel was checked for activity leakage and it was accounted for during the results processing. At the end of the exposure the radon activity from the drechsel was promptly transferred in a 50 L box and measured by reference radon monitor AlphaGUARD (Saphymo, Germany). This measurement and the volume ratio of the 180 mL drechsel and the 50 L box were used to estimate the radon activity concentration during the exposure. The Makrofol N foils were used for parallel estimate of the exposure activity concentration: they were placed in a LS glass vial filled with Filter Count LS cocktail (PerkinElmer, USA) and measured by a TDCR counter. The TDCR-measured activity and the well-known absorption properties of Makrofol N were used to estimate the radon activity concentration [25]. The two methods gave coherent results and the radon activity concentration, estimated as the average of the two methods, were C_0 = 151(13) MBq/m^3 (Oct.2020) and C_0 = 163(10) MBq/m^3 (Nov.2023). As the activity was introduced in the beginning of the exposure, it decreased during the exposure due to radioactive decay and leakage of radon from the drechsel. This decrease is described by exponential law $C_{out}(t) = C_0 e^{(-\lambda_{eff} t)}$ and the effective "decay" constant was estimated at λ_{eff} = 0.0093(7) h^{-1}.

After the exposure, the exposed PSDplastic samples were measured by different detectors:

- Two pieces with same thickness L = 526(5) μm were placed (Oct. 2020) at the cap of HPGe gamma-ray spectrometer (ORTEC, USA, relative efficiency 24.9% and resolution 1.9 keV for the 1332 keV gamma-line of ^{60}Co) and the decrease of the activity was followed by the gamma-lines 295 keV and 352 keV of ^{214}Pb. The HPGe detector efficiency for the given measurement geometry and energies of the gamma-lines was estimated by Monte Carlo simulations with the PENELOPE code [36]. That allowed us to obtain experimental data for $A_i(t_{d,i})$ which was fitted with the theoretical function (Eq. (2)) as described in Section 2.2 and to estimate both K and L_D.
- A piece with thickness L = 358(6) μm was placed (Oct. 2020) in the optical chamber of Polyphemus 1 and the decrease of the activity was followed by the alpha-line 7687 keV of ^{214}Po. As the detector efficiency was not known, the obtained count rate in the alpha-peak $n_{\alpha,i}(t_{d,i})$ was fitted with theoretical function (Eq. (2)) and only L_D was estimated. Additionally, these measurements were used to study the PSD properties of the PSDplastic.
- Pieces with thicknesses L = 302(5) μm (Oct.2020) and L = 283(9) μm (Nov.2023) were placed in a glass vial and the decrease of the activity was followed by gross alpha/beta-counting with a RackBeta 1219 LS-analyzer (Wallac, Finland). Similarly to the measurements by the Polyphemus 1, the counting rate in the full alpha/beta-spectra $n_{tot,i}(t_{d,i})$ was fitted to estimate L_D.
- Pieces with thicknesses L = 371(3) μm (Oct.2020) and L = 321(13) μm (Nov.2023) were placed in a glass vial filled to the top with Filter Count LS cocktail (PerkinElmer, USA) and measured with a triple-to-double coincidences ratio (TDCR) detector [37]. When the specimen is immersed in the scintillator and the vial is closed, the activity from the specimen redistributes between the specimen and the scintillator but it stays in the vial. That allows to measure precisely the absorbed activity by TDCR and to estimate K.
- The pieces used for PSD and α-spectra analysis were measured with the Polyphemus 1 and PERALS-spectrometer as described in the text.

4. Results

4.1. L_D and K of ^{222}Rn in the PSDplastic

The experimental data was processed as described in Section 3. The fitted data from the HPGe, Polyphemus 1 and RackBeta are shown in Figs. 4–6 and the results are summarized in Table 1. The obtained values are similar to other PS that we studied previously [20].

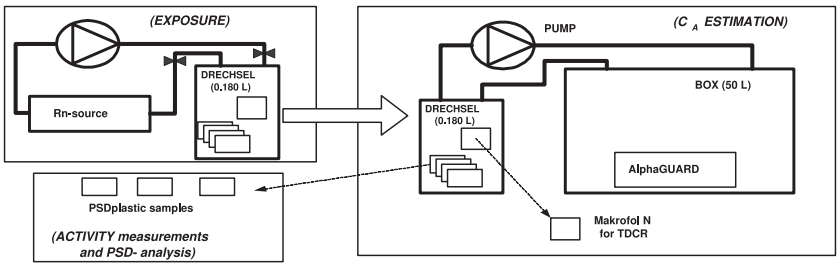

Fig. 3. Scheme of the experimental setup used for the exposure of PSDplastic samples.

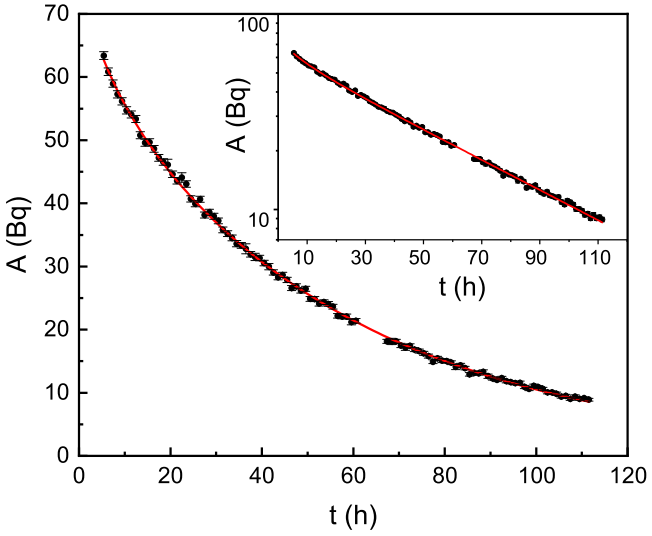

Fig. 4. Experimental study (points) of the radon desorption from the PSDplastic followed by gamma-spectrometry with a HPGe-detector. The solid line represents the data fitting with the theoretical function (Eq. (2)). The inset shows the same data in semi-logarithmic scale. The uncertainties of the experimental points are given at the level of 1σ.

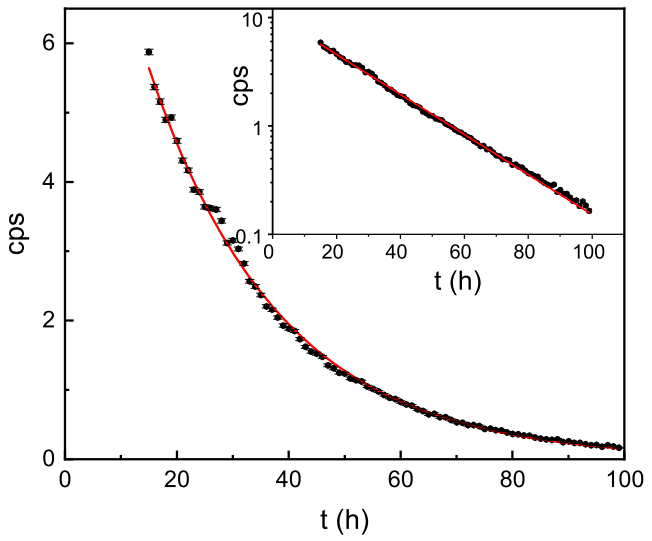

Fig. 5. Experimental study (points) of the radon desorption from the PSDplastic followed by Polyphemus 1. The solid line represents the data fitting with the theoretical function (Eq. (2)). The inset shows the same data in semi-logarithmic scale. The uncertainties of the experimental points are given at the level of 1σ.

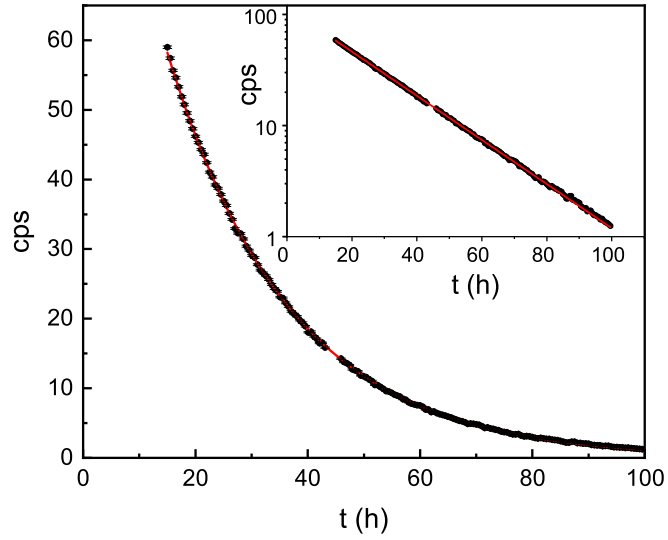

Fig. 6. Experimental study (points) of the radon desorption from the PSDplastic followed by gross alpha/beta-counting with the RackBeta LS-counter. The solid line represents the data fitting with the theoretical function (Eq. (2)). The inset shows the same data in semi-logarithmic scale. The uncertainties of the experimental points are given at the level of 1σ.

Table 1
Partition coefficient K and diffusion length L_D of ^{222}Rn in PSDplastic at T = 20(1) °C estimated from the measurements with different detectors. The thicknesses L of the PSDplastic plates measured on each detector are also given. In the case of the HPGe 2 pieces with the same thickness were used. The uncertainties are at the level of 1σ.

Measurement date	Detector	L (μm)	K	L_D (μm)
October 2020	HPGe	526(5)	11.4(15)	195(20)
October 2020	TDCR	371(3)	9.7(9)	–
October 2020	Polyphemus 1	368(6)	–	245(25)
October 2020	RackBeta	302(5)	–	216(22)
November 2023	TDCR	321(13)	10.18(92)	–
November 2023	RackBeta	283(9)	11.9(10)	239(24)
Average			10.6(11)	224(23)

4.2. PSD measurements of ^{222}Rn absorbed in PSDplastic

The spectra presented here were obtained with the Polyphemus 1 and PERALS detectors. In the Polyphemus 1 measurements 5 of the sides of a rectangular piece of the PSDplastic were covered with reflective foil. The sixth side was attached to the PMT window using silicon optical grease. This was done for two reasons: 1. to optimize the energy resolution; 2. to be consistent with previous measurements made with this PS and investigate changes over time. The four spectra simultaneously obtained with the nanoPSD digital spectrometer are the TIPS, raw $\alpha+\beta$ spectrum and the separated β and α spectra (see Fig. 7).

In the TIPS spectrum there are two well separated peaks - one formed by the β-particles which have lower TIPS values and the other formed by the α-particles with higher TIPS values. The excellent PSD

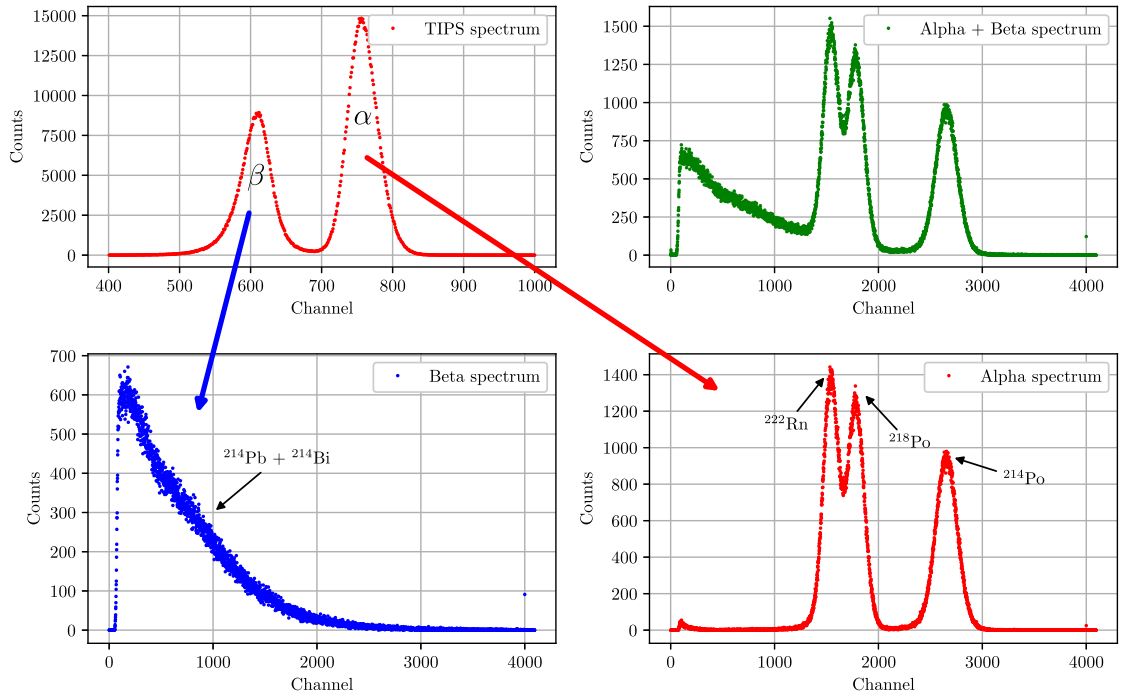

Fig. 7. Polyphemus1 measurement of ^{222}Rn absorbed in the PSDplastic. Radon-222 is in secular equilibrium with its short-lived decay products and their contribution to the different spectra is indicated.

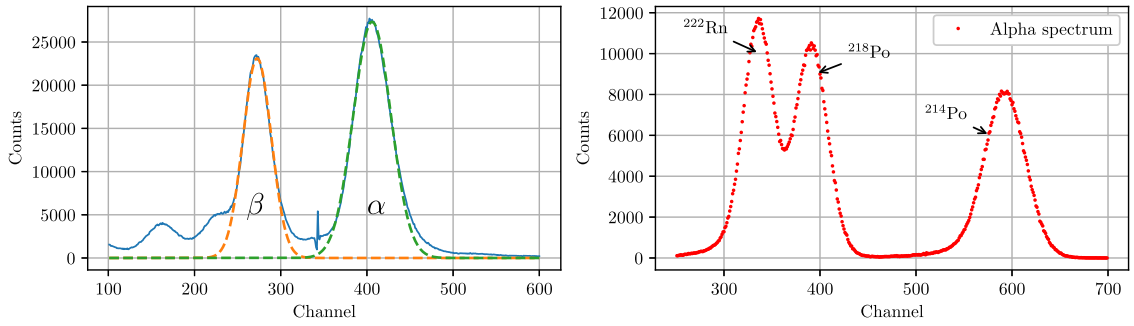

Fig. 8. Measurements with PERALS. TAC (left) and α (right) spectra of ^{222}Rn and its progeny in the PSDplastic.

capabilities of the PSDplastic are verified by the lack of α-peaks in the β-spectrum and the lack of beta-continuum in the α-spectrum (see Fig. 7). Similar excellent separation with this PS was observed previously [37]. The PSD threshold position in the PSD TIPS spectrum is set to channel 690 - in the minimum between the two peaks. The negligible cross-talk between the α and β channels allows to apply models to fit the α-spectrum and obtain reliable data for the energy resolution of this PS.

In the case of PERALS measurements, a small sample of the PSD plastic is directly inserted into the sample vial (see Fig. 2). The time-to-amplitude spectrum (TAC) of PERALS is displayed on the left in Fig. 8. The green and orange lines in the figure represent the contributions of alpha and beta particles to the TAC spectrum, respectively. The blue line depicts the acquired TAC spectrum. The selected threshold for PSD discrimination is indicated by an oscillation in the TAC spectrum (around channel 340). The TAC spectrum demonstrates the excellent PSD characteristics of the PSD plastic. Additionally, the α-spectrum of PERALS shows no contribution from the beta continuum, indicating negligible beta-to-alpha cross-talk.

The temporal stability of the energy resolution of the PSD plastic was investigated through periodic measurements over time. To conduct this study, small samples were cut from the same piece of PSD plastic, polished, and then placed in the detectors for measurement. For each measurement session, a new piece of PSD plastic was cut, with the initial measurement commencing in 2017. During intervals between measurements, the scintillator was stored in a dark, dry place under room conditions. The results are shown in Table 2. This study was necessary, taking into account that most recent PSDplastics suffer from various ageing phenomena: deformation, whitening, softening or even oxidation such as all plastics which contain 2,5-diphenyloxazole as the highly concentrated primary fluorophore.

Table 2
Energy resolution from measurements made with PERALS and Polyphemus 1 at five different dates.

Time of measurement	Detector	^{222}Rn R, %	^{218}Po R, %	^{214}Po R, %
January 2019	PERALS	5.80(8)	5.83(7)	5.76(6)
November 2020	PERALS	5.71(15)	5.66(8)	5.55(13)
November 2023	PERALS	5.80(10)	5.75(10)	5.60(10)
December 2017	Polyphemus 1	6.41(8)	6.44(7)	6.50(6)
June 2021	Polyphemus 1	5.59(23)	5.90(20)	5.82(33)

The results presented in Table 2 show no signs of deterioration in the energy resolution of the PSDplastic over time. There are no apparent signs of aging or other adverse phenomena identified from

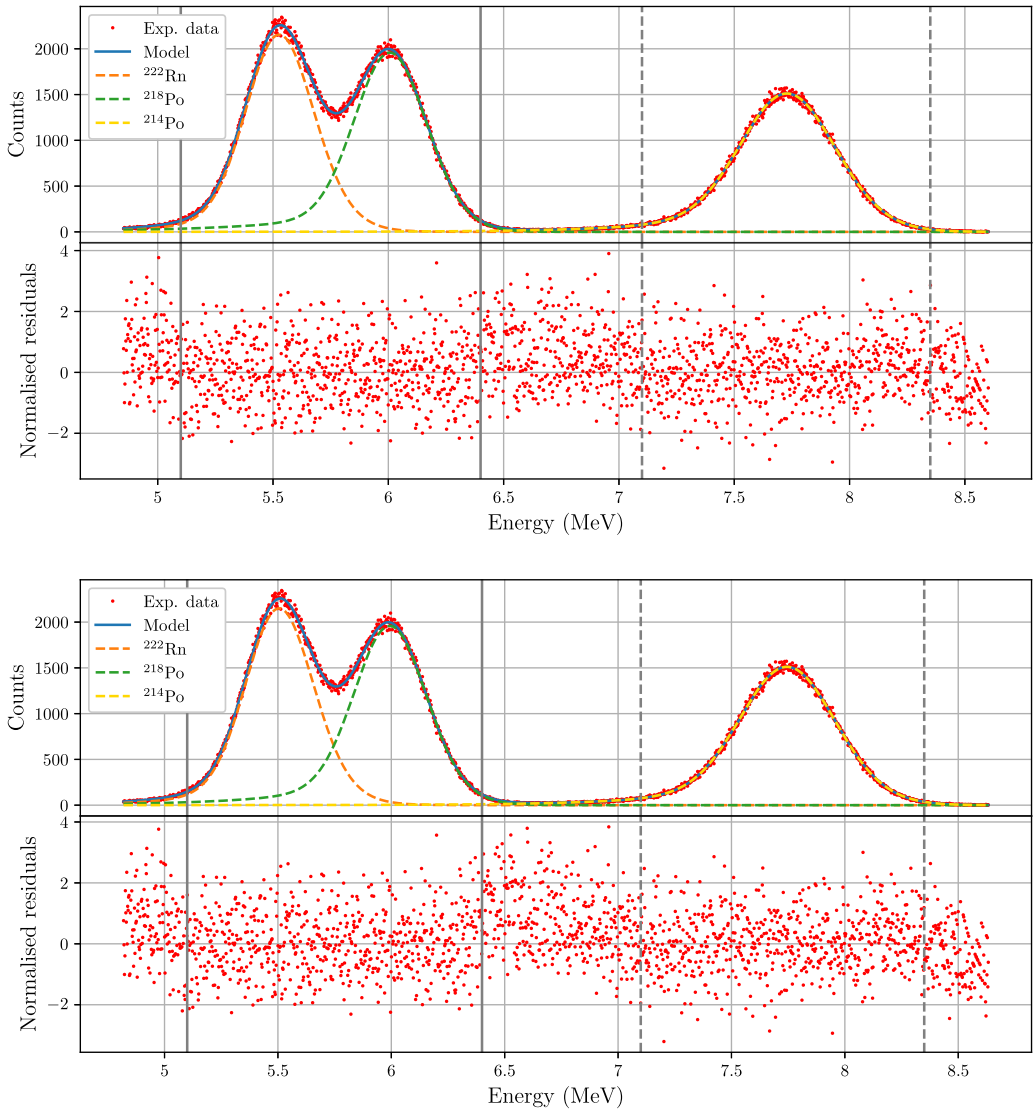

Fig. 9. Alpha spectra, obtained with the Polyphemus 1 system in 2017. Top: fit with 12 exponential coefficients (Eq. (8)). Bottom: fit with 4 exponential coefficients (Eq. (9)).

the measured energy resolutions over the five-year period, which consistently agree within the estimated uncertainties. The only exception is the initial energy resolution measurement with Polyphemus 1 in 2017. Unfortunately, this measurement was conducted with a large piece of PSDplastic (12×13 mm^2), affecting the measured energy resolution due to non-uniformities in the spatial response of the photocathode of the PMT (for more details, see [31]). At that time, we were unaware that both the size of the PS and its position on the PMT significantly influence the obtained α-spectra and their energy resolution. Subsequent measurements from 2019 onward were made with a 5×5 mm^2 piece in the center of the PMT photocathode. The results obtained with the PERALS and Polyphemus 1 spectrometers indicate that the studied scintillator has maintained its energy resolution over time. Additionally, the mechanical strength and optical transparency of the PSDplastic remain intact.

4.3. Analysis of the alpha-spectra of ^{222}Rn absorbed in PSDplastic

Owing to the remarkable PSD capabilities of the PSDplastic, the α- and β-spectra of ^{222}Rn absorbed in it are well-separated, and there is practically no cross-talk between them. This facilitates the application of analytical models to approximate the α-spectra. The spectra that were analyzed were acquired when ^{222}Rn has reached an almost steady-state distribution inside the PSD plastic (typically after more than 36 h after the end of the exposure) and in secular equilibrium between ^{222}Rn and its decay products. Two separate regions were analyzed: region A— the interval of channels that includes the ^{222}Rn and ^{218}Po α-peaks, and region B— the interval that includes the ^{214}Po peak. For all processed spectra, the beginning and the end of each region were the same. In total 25 spectra were analyzed and typical examples of the obtained results are shown in Figs. 9 (Polyphemus 1) and 10 (PERALS).

The plots of the normalized residuals in Figs. 9 and 10 indicate that both models approximate well the experimental spectra in regions A and B. In order to compare the models in a quantitative manner, the statistical criteria AIC and BIC (Section 2.4) were applied and the results are shown in Tables 3 (Polyphemus 1) and 4 (PERALS).

From the obtained results, it can be argued that the model with 4 exponential coefficients (Eq. (9)) provides values of the reduced χ^2_{red} that are either better or comparable to the model with 12 exponential coefficients. The statistical criterion AIC, penalizing models with more than the optimal set of parameters, favors the 4-exponential coefficient model. The weights w_i(AIC) indicate that, in nine out of ten cases, the model with the smaller number of parameters is more plausible. The weights w_i(BIC), which apply an even greater penalty for models with more parameters, confirm the results of the AIC weights.

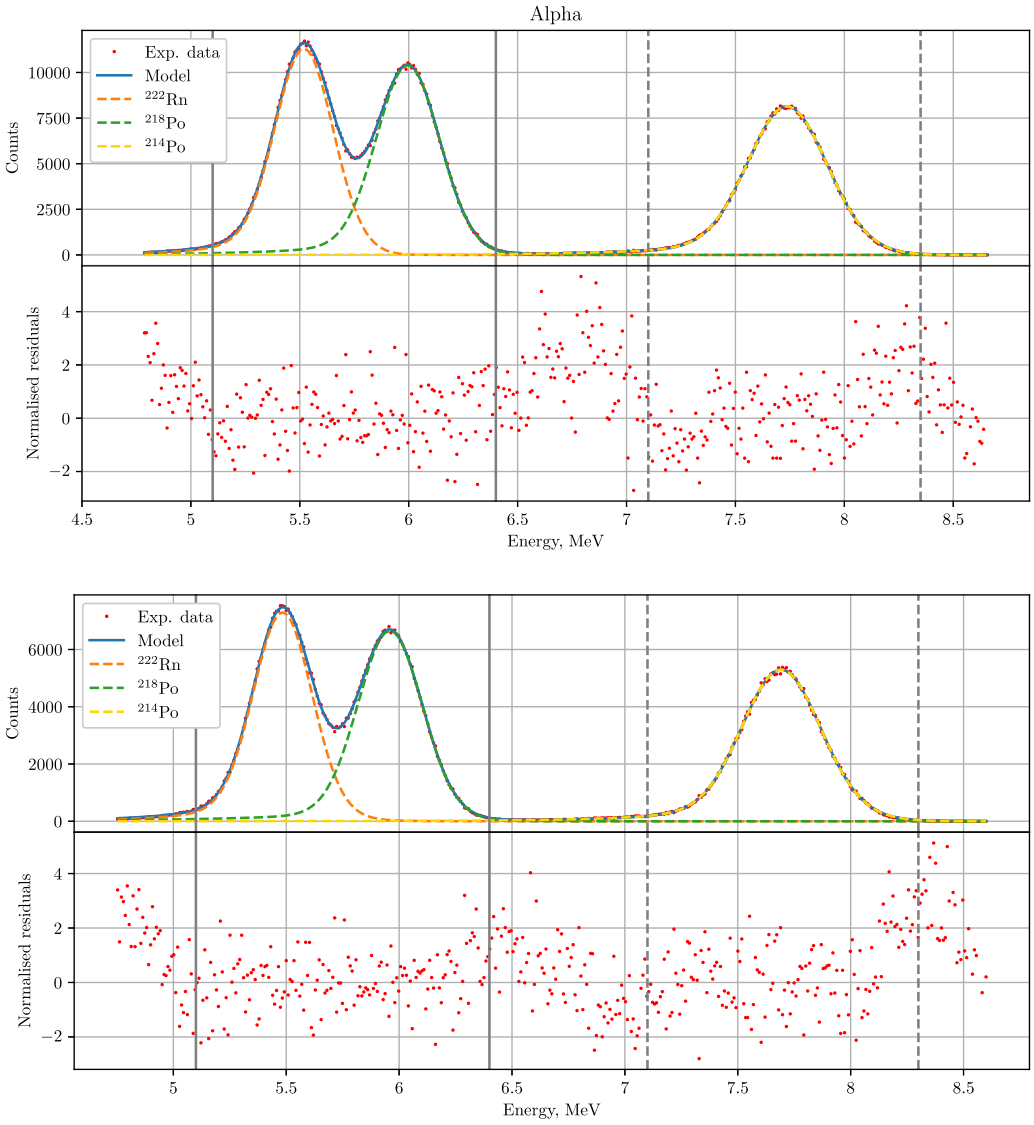

Fig. 10. Alpha spectra, obtained with the PERALS system in 2023. Top: fit with 12 exponential coefficients (Eq. (8)). Bottom: fit with 4 exponential coefficients (Eq. (9)).

Table 3
Statistical criteria of the 12 and 4 exponential parameter fits of spectra obtained with the Polyphemus 1 system.

Date	Region	Model	χ^2_{red}	$w_i(AIC)$	$w_i(BIC)$
Dec 2017	A	12 exp	1.08	0.005	6E−08
		4 exp	1.07	0.995	1
	B	12 exp	0.84	1E−05	2E−08
		4 exp	0.81	1	1
Jun 2021	A	12 exp	1.18	1	0.994
		4 exp	1.23	6E−08	6E−03
	B	12 exp	1.36	1E−18	1E−21
		4 exp	1.23	1	1

Table 4
Statistical criteria of the 12 and 4 exponential parameter fits of spectra obtained with the PERALS system.

Date	Region	Model	χ^2_{red}	$w_i(AIC)$	$w_i(BIC)$
Jan 2019	A	12 exp	1.3	0.2	1E−05
		4 exp	1.3	0.8	1
	B	12 exp	1.3	0.7	1E−02
		4 exp	1.4	0.3	1
Nov 2020	A	12 exp	1.3	0.98	9E−02
		4 exp	1.5	0.02	1
	B	12 exp	2.2	3E−05	5E−07
		4 exp	1.9	1	1
Nov 2023	A	12 exp	1.2	4E−02	2E−05
		4 exp	1.2	1	1
	B	12 exp	1.2	5E−06	5E−08
		4 exp	1.0	1	1

The comparison between the models with 12 and 4 exponential coefficients suggests that, based on the physics of the detection process, the number of parameters can be optimized in a way that a model with fewer parameters results in a better approximation.

5. Conclusions

A plastic scintillator developed for neutron/gamma PSD was studied, and its ^{222}Rn absorption properties, as well as its capability for alpha/beta PSD, were investigated. It has been demonstrated that this plastic scintillator also possesses remarkable alpha/beta PSD properties, good energy resolution, and maintains these properties over a storage time of five years.

The partition coefficient and diffusion length of ^{222}Rn in the plastic scintillator were determined. The study showed that the absorption of radon in the plastic scintillator could facilitate studies of alpha/beta PSD and energy resolution properties, as the absorbed radon and its progeny represent a mixed alpha/beta source inside the scintillator.

An improvement to the method for analyzing alpha spectra obtained after PSD with this scintillator is proposed. The improved method uses fewer parameters and demonstrates superior or equivalent performance compared to the original approach. The significant advantage of the new model lies in considering the influencing physical factors, which can lead to satisfactory results with a more parsimonious model.

CRediT authorship contribution statement

Vladislav Todorov: Writing – original draft, Validation, Software, Methodology, Investigation, Formal analysis, Data curation. **Strahil Georgiev:** Writing – original draft, Validation, Methodology, Investigation, Formal analysis, Data curation. **Matthieu Hamel:** Writing – review & editing, Validation, Supervision, Resources, Methodology, Investigation, Formal analysis, Data curation, Conceptualization. **Chavdar Dutsov:** Writing – review & editing, Methodology, Investigation, Formal analysis. **Benoit Sabot:** Writing – review & editing, Investigation, Formal analysis, Data curation. **Ivelina Dimitrova:** Writing – review & editing, Investigation, Formal analysis, Data curation. **Krasimir Mitev:** Writing – original draft, Validation, Supervision, Resources, Project administration, Methodology, Investigation, Funding acquisition, Formal analysis, Data curation, Conceptualization.

Declaration of competing interest

Part of this work is patented under priority number FR1352072.

The authors declare that they have no known competing financial interests or personal relationships that could have appeared to influence the work reported in this paper.

Data availability

Data will be made available on request.

Acknowledgments

This work received support by the European Union NextGenerationEU, through the National Recovery and Resilience Plan of the Republic of Bulgaria, project N∘ BG-RRP-2.004-0008-C01.

References

[1] G.T. Wright, Scintillation decay times of organic crystals, Proc. Phys. Soc. Sect. B 69 (3) (1956) 358–372, http://dx.doi.org/10.1088/0370-1301/69/3/311.

[2] F.D. Brooks, R.W. Pringle, B.L. Funt, Pulse shape discrimination in a plastic scintillator, IRE Trans. Nucl. Sci. 7 (2/3) (1960) 35–38, http://dx.doi.org/10.1109/tns2.1960.4315733.

[3] D.L. Horrocks, Interaction of fission fragments with organic scintillators, Rev. Sci. Instrum. 34 (9) (1963) 1035–1040, http://dx.doi.org/10.1063/1.1718650.

[4] J.B. Birks, The Theory and Practice of Scintillation Counting, Pergamon Press, Oxford, 1964.

[5] S. Nyibule, E. Henry, W.U. Schröder, J. Tõke, L. Acosta, L. Auditore, G. Cardella, E. De Filippo, L. Francalanza, S. Gìani, T. Minniti, E. Morgana, E.V. Pagano, S. Pirrone, G. Politi, L. Quattrocchi, F. Rizzo, P. Russotto, A. Trifirò, M. Trimarchi, Radioluminescent characteristics of the EJ 299-33 plastic scintillator, Nucl. Instrum. Methods Phys. Res. A 728 (2013) 36–39, http://dx.doi.org/10.1016/j.nima.2013.06.020.

[6] P. Blanc, M. Hamel, C. Dehé-Pittance, L. Rocha, R.B. Pansu, S. Normand, Neutron/gamma pulse shape discrimination in plastic scintillators: Preparation and characterization of various compositions, Nucl. Instrum. Methods Phys. Res. A 750 (2014) 1–11, http://dx.doi.org/10.1016/j.nima.2014.02.053.

[7] M. Hamel (Ed.), Plastic Scintillators: Chemistry and Applications, in: Topics in Applied Physics, vol. 140, Springer, Cham, 2021, http://dx.doi.org/10.1007/978-3-030-73488-6.

[8] F. Bisaro, A. Inial, J. Gatignol, F. Allix, A. Stallivieri, J.-L. Renaud, L. Achouri, M. Parlog, F. Delaunay, T.-N. Pham, M. Hamel, S. Gaillard, Plastic scintillators with 1-phenyl-3-(mesityl)-2-pyrazoline as unique fluorophore for efficient neutron/gamma pulse shape discrimination, Nucl. Instrum. Methods Phys. Res. A 1030 (2022) 166469, http://dx.doi.org/10.1016/j.nima.2022.166469.

[9] H. Bagán, A. Tarancón, G. Rauret, J.F. García, Alpha/beta pulse shape discrimination in plastic scintillation using commercial scintillation detectors, Anal. Chim. Acta 670 (2010) 11–17, http://dx.doi.org/10.1016/j.aca.2010.04.055.

[10] L.M. Santiago, H. Bagán, A. Tarancón, J.F. García, Synthesis of plastic scintillation microspheres: Alpha/beta discrimination, Appl. Radiat. Isot. 93 (2014) 18–28, http://dx.doi.org/10.1016/j.apradiso.2014.04.002.

[11] K.K. Mitev, Measurement of ^{222}Rn by absorption in plastic scintillators and alpha/beta pulse shape discrimination, Appl. Radiat. Isot. 110 (2016) 236–243, http://dx.doi.org/10.1016/j.apradiso.2016.01.027.

[12] E. Pelay, A. Tarancón, K. Mitev, C. Dutsov, S. Georgiev, L. Tsankov, J.F. García, Synthesis and characterisation of scintillating microspheres made of polystyrene/polycarbonate for ^{222}Rn measurements, J. Radioanal. Nucl. Chem. 314 (2) (2017) 637–649, http://dx.doi.org/10.1007/s10967-017-5488-3.

[13] Yantel, nanoPSD, product information, 2022, Online; accessed 01-Aug-2022. URL https://www.yantel.com/products/nanopsd/.

[14] K. Mitev, V. Jordanov, M. Hamel, C. Dutsov, S. Georgiev, P. Cassette, Development of a portable scintillation spectrometer with alpha-/beta- and neutron-/gamma- pulse-shape discrimination capabilities, in: 2018 IEEE Nuclear Science Symposium and Medical Imaging Conference Proceedings, NSS/MIC, IEEE, 2018, http://dx.doi.org/10.1109/NSSMIC.2018.8824692.

[15] Y. Morishita, A. Di Fulvio, S.D. Clarke, K.J. Kearfott, S.A. Pozzi, Organic scintillator-based alpha/beta detector for radiological decontamination, Nucl. Instrum. Methods Phys. Res. A 935 (2019) 207–213, http://dx.doi.org/10.1016/j.nima.2019.04.024.

[16] Y. Morishita, Y. Ye, L. Mata, S.A. Pozzi, K.J. Kearfott, Radon measurements with a compact, organic-scintillator-based alpha/beta spectrometer, Radiat. Meas. 137 (2020) 106428, http://dx.doi.org/10.1016/j.radmeas.2020.106428.

[17] T.J. Hajagos, D. Kishpaugh, Q. Pei, Pulse shape discrimination properties of plastic scintillators incorporating a rationally designed highly soluble and polymerizable derivative of 9 10-diphenylanthracene, Nucl. Instrum. Methods Phys. Res. A 825 (2016) 40–50, http://dx.doi.org/10.1016/j.nima.2016.04.029, URL https://www.sciencedirect.com/science/article/pii/S0168900216301887.

[18] D. Pressyanov, K. Mitev, S. Georgiev, I. Dimitrova, Sorption and desorption of radioactive noble gases in polycarbonates, Nucl. Instrum. Methods Phys. Res. A 598 (2009) 620–627, http://dx.doi.org/10.1016/j.nima.2008.09.044.

[19] K. Mitev, I. Dimitrova, A. Tarancón, D. Pressyanov, L. Tsankov, T. Boshkova, S. Georgiev, R. Sekalova, J.F. García, Pilot study of the application of plastic scintillation microspheres to Rn-222 detection and measurement, IEEE Trans. Nucl. Sci. 63 (2) (2016) 1209–1217, http://dx.doi.org/10.1109/TNS.2016.2530857.

[20] K. Mitev, C. Dutsov, S. Georgiev, L. Tsankov, T. Boshkova, Study of ^{222}Rn absorption and detection properties of EJ-212 and BC-400 plastic scintillators, IEEE Trans. Nucl. Sci. 64 (6) (2017) 1592–1598, http://dx.doi.org/10.1109/TNS.2017.2699041.

[21] G.H.V. Bertrand, M. Hamel, S. Normand, F. Sguerra, Pulse shape discrimination between (fast or thermal) neutrons and gamma rays with plastic scintillators: State of the art, Nucl. Instrum. Methods Phys. Res. A 776 (2015) 114–128, http://dx.doi.org/10.1016/j.nima.2014.12.024.

[22] E. Montbarbon, M.-N. Amiot, D. Tromson, S. Gaillard, C. Frangville, R. Woo, G.H.V. Bertrand, R.B. Pansu, J.-L. Renaud, M. Hamel, Large irradiation doses can improve the fast neutron/gamma discriminating capability of plastic scintillators, Phys. Chem. Chem. Phys. 19 (41) (2017) 28105–28115, http://dx.doi.org/10.1039/c7cp04034b.

[23] D. Pressyanov, S. Georgiev, I. Dimitrova, K. Mitev, T. Boshkova, Determination of the diffusion coefficient and solubility of radon in plastics, Radiat. Prot. Dosim. 145 (2–3) (2011) 123–126, http://dx.doi.org/10.1093/rpd/ncr069.

[24] D. Pressyanov, K. Mitev, I. Dimitrova, S. Georgiev, Solubility of krypton, xenon and radon in polycarbonates. application for measurement of their radioactive isotopes, Nucl. Instrum. Methods Phys. Res. A 629 (2011) 323–328, http://dx.doi.org/10.1016/j.nima.2010.11.112.

[25] K. Mitev, P. Cassette, S. Georgiev, I. Dimitrova, B. Sabot, T. Boshkova, I. Tartès, D. Pressyanov, Determination of ^{222}Rn absorption properties of polycarbonate foils by liquid scintillation counting. application to ^{222}Rn measurements, Appl. Radiat. Isot. 109 (2016) 270–275, http://dx.doi.org/10.1016/j.apradiso.2015.11.047.

[26] K. Mitev, P. Cassette, I. Tartès, S. Georgiev, I. Dimitrova, D. Pressyanov, Diffusion lengths and partition coefficients of ^{131m}Xe and ^{85}Kr in Makrofol N and Makrofol DE polycarbonates, Appl. Radiat. Isot. 134 (2018) 269–274, http://dx.doi.org/10.1016/j.apradiso.2017.07.023.

[27] S. Georgiev, K. Mitev, C. Dutsov, T. Boshkova, I. Dimitrova, Partition coefficients and diffusion lengths of ^{222}Rn in some polymers at different temperatures, Int. J. Environ. Res. Public Health 16 (22) (2019) 4523, http://dx.doi.org/10.3390/ijerph16224523.

[28] V.T. Jordanov, Pile-up real time pulse-shape discrimination based on ballistic deficit measurement and digital time-invariant pulse shaping, in: 2018 IEEE Nuclear Science Symposium and Medical Imaging Conference Proceedings, NSS/MIC, IEEE, 2018, http://dx.doi.org/10.1109/nssmic.2018.8824502.

[29] ORDELA Inc., Perals® simplified environmental alpha spectrometry, 2017, online; accessed 01-Aug-2022. URL https://ordelacom.files.wordpress.com/2017/01/peralsc2ae-color-brochure-revised.pdf.

[30] K. Mitev, P. Cassette, Radioactive noble gas detection and measurement with plastic scintillators, in: M. Hamel (Ed.), Plastic Scintillators, in: Topics in Applied Physics, vol. 140, Springer, Cham, 2021, pp. 385–423, http://dx.doi.org/10.1007/978-3-030-73488-6_11.

[31] V.T. Todorov, C.C. Dutsov, P. Cassette, K.K. Mitev, Effects of the photocathode non-uniformity on radon measurements by plastic scintillation spectrometry, J. Radioanal. Nucl. Chem. 331 (2022) 3249–3258, http://dx.doi.org/10.1007/s10967-022-08362-6.

[32] M.-M. Bé, V. Chisté, C. Dulieu, E. Browne, V. Chechev, N. Kuzmenko, F. Kondev, A. Luca, M. Galán, A. Pearce, X. Huang, Monographie BIPM-5: Table of Radionucleides, Vol. 4, Bureau International des Poids et Mesures, France, ISBN: 92-822-2230-6, 2008, URL https://www.bipm.org/en/publications/monographies.

[33] W.H. Press, S.A. Teukolsky, B.P. Flannery, W.T. Vetterling, Numerical Recipes in FORTRAN 77: The Art of Scientific Computing, Vol. 1, Cambridge University Press, 1992.

[34] K.P. Burnham, D.R. Anderson, Model Selection and Multimodel Inference: A Practical Information-Theoretic Approach, second ed., Springer, 2007.

[35] R. Rossi, A. Murari, P. Gaudio, M. Gelfusa, Upgrading model selection criteria with goodness of fit tests for practical applications, Entropy 22 (4) (2020) 447, http://dx.doi.org/10.3390/e22040447.

[36] J. Sempau, J.M. Fernández-Varea, E. Acosta, F. Salvat, Experimental benchmarks of Monte Carlo code PENELOPE, Nucl. Instrum. Methods Phys. Res. B 207 (2003) 107–123, http://dx.doi.org/10.1016/S0168-583X(03)00453-1.

[37] K. Mitev, P. Cassette, V. Jordanov, H.R. Liu, C. Dutsov, Design and performance of a miniature TDCR counting system, J. Radioanal. Nucl. Chem. 314 (2) (2017) 583–589, http://dx.doi.org/10.1007/s10967-017-5451-3.